XEUS Focal Plane Accommodation Study – WP 1220: Shielding and straylight analysis report

INAF/ IASF-Bologna Internal Report n. 449 / 2006

L. Foschini[(1)], V. Fioretti[(1,2)]

[(1)]INAF/ IASF-Bologna, Italy
[(2)]Dipartimento di Astronomia, Università di Bologna, Italy

Change history

Version	Date	Notes
1.0	Nov 2nd, 2006	1st Issue

1. Introduction and aim

The continuum sensitivity of an X-ray focussing telescope, defined as the minimum detectable flux F_{min}, can be expressed as[1]:

$$F_{min} = \text{const} \cdot \frac{\sqrt{B \cdot A_D}}{A_{Eff}},$$

where A_{Eff} is the telescope effective area, A_D the telescope point spread function (PSF) projected at the focal plane, and B is the background. The background is defined here as the sum of all "detected" signals, which are not due to the observed source. From the above equation it is clear the importance of the necessity of minimizing the background in order to reach deep sensitivity levels, which is one of the key scientific requirements of the XEUS Mission.
The background can be classified into two broad classes, depending upon the primary particle origin: (i) Hadron induced, and (ii) Photon induced.

The particle (hadron) induced component concerns the signals caused by the interaction of high energy particles (mainly protons and electrons) with the spacecraft, telescope, and detectors structures. According to the involved interactions and type of signals caused at the detectors, it can be classified into the following main classes:

- Prompt emission:

These are signals caused by the spallation effects of incident cosmic rays on the spacecraft. Whether the prompt cosmic-ray component of the background dominates or it is even significant depends on the chosen orbit (LEO, HEO, L2, etc...), and the material surrounding the detector. In general this component can be handled with by means of an active coincidence veto system.

- Delayed emission:

It is due to materials in the spacecraft excited by the incident cosmic ray flux. Therefore the delayed component is both slowly varying, highly specific to the instrument and, depending on the half-lives of the materials involved, can build-up asymptotically over a much longer time scale than any prompt cosmic ray. It is then not possible to "kill" it by means of active anticoincidence, and implies a careful modelling and calibration.

- Solar flares induced emission:

Solar energetic particles can cause impulsive or gradual background increase depending on the solar activity, orbit and aspect angle.

- Magnetospheric trapped particles:

Protons and electrons constrained within the Earth magnetic fields can cause local and variable background signals. This component is thought to be the responsible of the "soft proton flares" noise recorded by *Chandra* and *XMM-Newton*. In these cases, the soft (tens to hundreds of keV) protons are funnelled through the mirror shells down to the detection plane causing signals virtually indistinguishable from valid events. To minimize this effect, magnetic brooms are foreseen in order to deflect electrons outside the detection plane. Moreover, after the *Chandra* and *XMM-Newton* experiences, the possibility to implement also a proton diverter is under study.

The *photon* component can be further subdivided into four main classes: (a) single- or zero-reflection events through the mirror shells, (b) aperture flux from directions not covered by the passive or active shields (stray-light), (c) shield leakage or fluorescence emission, (d) Compton scattered photons from the mirror shells. Components (a) and (d), depending on the mirror optics design, do not concern the telescope focal plane accommodation and will not addressed in this note.

[1] The equation considers the statistical limit of F_{min} in the absence of systematic effects. The constant thus includes, among all other detector and mirror parameters (like detector area, observing time, etc..), also the statistical significance of the detection.

The aperture flux background component is caused by the cosmic X-ray background (CXB) that reaches the detector without being focussed, i.e. from directions outside the optics shells assembly. In the case of a formation flight telescope like XEUS, the potential importance of this component is increased by the practical impossibility of having the canonical "tube" optically isolating the mirror from the focal plane assemblies. As will be explained in detail in the following Sections, we will assume a *"perfect"* shielding system geometry, i.e. completely covering all directions outside the telescope FOV. This ensures the minimization of the CXB induced background component, which is of key importance also because the hadronic (particle) background component is instead very uncertain and depends upon several independent factors like telescope orbit, solar activity, and so on, and will be exactly quantified only when the mission is in orbit.

This note is a first analysis report concerning the possible optimization of the XEUS detector payload accommodation taking into account the necessity of background minimization. For this reason, particular attention is given to the detector payload design characteristics which can direct impact on the expected main background components: i.e. shielding geometry, thickness and composition.

In Section 2 a brief analysis review of the trade-off phase space is given, while in Section 3 the possible implementation solutions for the XEUS payload are described. In Section 4 the possibility of implementing a magnetic broom to deflect charged particles is also addressed.

2. Shield design optimization philosophy

The key design parameters of the detectors shield can be summarized as: geometry, thickness, and composition. The possible science-driven configurations will have to be checked in terms of mechanical and thermal stability, and then verified against the available mass and power budgets.

The geometry of the shielding system is required, at least in a first conservative approach, to completely shield the detector from unwanted aperture flux. Figure 1 shows a simplified conceptual design of this approach in the case of a simple collimator (more complex solutions will be presented in Section 3).

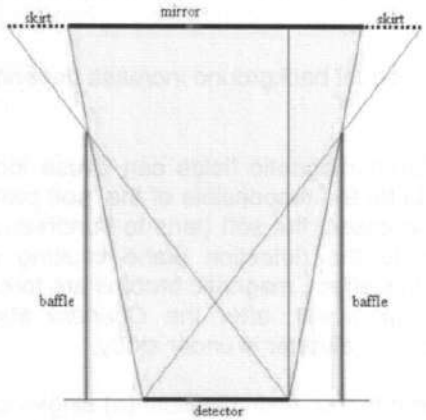

Figure 1: Simplified conceptual design of the baffle and skirt geometrical configuration. The DSC baffle (thick green lines) and the MSC skirt (dotted lines) allow the detector (thick black line on the bottom) to "see" only those directions (pink area) that correspond to the photons focused by the mirror system (thick black line on the top)

The thickness of the shield needs to be optimized against the required absorbing power. A narrow parallel monochromatic X-ray beam of intensity I_0 passing through a sample of thickness t will get a reduced intensity I according to the following well known expression:

$$\frac{I}{I_0} = e^{-\mu t} = 1 - eff$$

where μ is the linear absorption coefficient *[cm^{-1}]*, and *eff* is the efficiency of absorption.

The absorption coefficient depends on the types of atoms, the density ρ of the material and the total cross section for each atom σ_{tot}, which represents the probability that a photon interacts with a single atom and depends on the energy of the photon and on the interaction mechanism. It is sometimes useful to use the mass absorption coefficient, μ_ρ which is defined as μ/ρ.

At energies below about 100 keV, i.e. within the XEUS instruments operating ranges, the photoelectric effect is the dominant radiation-matter interaction process. In this process the interaction between the X-ray and the entire atom results in the absorption of the radiation and the ejection of an electron with kinetic energy $E_{e^-}=E_{phot}-E_{bind}$, where E_{phot} is the incident photon energy, and E_{bind} is the electron binding energy. The atom is left in an excited state and a second electron from a more external shell can replace the missing one, with an emission of an X-ray or Auger electron. The most tightly bound electrons have the greatest probability of absorbing X-rays and ≈80% of absorption occurs in the K (innermost) shell, as long as $E_{phot}>E_{bind}(K_{shell})$.
This process generates K_α emission (fluorescence radiation) of characteristic energy which depends upon the materials. The K_α line energies for the common materials used as absorbers are shown in Table 1. If the K_α characteristic energy falls within the detector energy range, then the shield must foresee, on top of the "main absorber", one or more layers ("grading"), in order to minimize the effect of (i.e. absorb) the K_α emission lines.

Material	Z	Density [g cm^{-3}]	K_α energy [keV]
Pb	82	11.35	74.97
W	74	19.30	59.32
Ta	73	16.65	57.5
C	6	1.700	0.277

Table 1: Shielding systems main absorber material properties.

It is also possible to use Au as the main absorber. Au has physical properties close to W (Z=79, density = 19.32 g/cm^3, and Kα energy = 68.8 keV), so that the implied grading material is not very different from what is necessary for W.
The thickness t is then given by:

$$t = \frac{-\ln(1-\mathrm{eff})}{\mu(E_{phot})}$$

where $\mu(E_{phot})$ depends upon the incident photon energy chosen for the thickness optimisation. The above equation shows the thickness corresponding to an attenuation factor equal to *(1-eff)* and, assuming a beam perpendicular to the baffle wall, it is the effective thickness of absorbing material.

In order to evaluate the necessary thickness, two possible shield thickness and composition optimizations have been explored.

A. To reach an absorption >99% ($I/I_0<1\%$) at 14 keV (40 keV for HXC)
B. To reach an absorption equivalent to one attenuation length ($I/I_0<e^{-1}\approx37\%$) at 28 keV (n.a. to HXC)

Given the energy range of the detectors foreseen for XEUS, two shield compositions have been considered for the present analysis: one for all instruments except HXC, and one for HXC alone.

2.1. Shield composition optimization for all instruments except HXC

Optimization approaches A and B described above have been followed considering two possible shield compositions: one with Aluminium (Al) as absorber plus Carbon (C) as grading layer, and one with C only. The thickness of the grading layer are calculated in order to reach an efficiency *eff=99%* at the energy of the preceding K_α emission line. The results are as follows:

Option A (I/I_0<1% at 14 keV) – Al+C:		*Option A (I/I_0<1% at 14 keV) – C only:*	
Al thickness:	1.71 mm	C thickness:	30.1 mm
C thickness (grading):	0.04 mm	C column density:	5.12 g/cm^2
Total (Al+C) thickness:	1.74 mm		
Al column density:	0.46 g/cm^2		
C column density:	0.0066 g/cm^2		
Total (Al+C) column density:	0.47 g/cm^2		

Option B (I/I_0<e^{-1} at 28 keV) – Al+C:		*Option B (I/I_0<e^{-1} at 28 keV) – C only:*	
Al thickness:	2.85 mm	C thickness:	21.01 mm
C thickness (grading):	0.008 mm	C column density:	3.57 g/cm^2
Total (Al+C) thickness:	2.86 mm		
Al column density:	0.77 g/cm^2		
C column density:	0.0014 g/cm^2		
Total (Al+C) column density:	0.77 g/cm^2		

2.2. Shield composition optimization for HXC

The explored compositions foresee as main absorber: Lead (Pb), Tungsten (W), Tantalum (Ta), or Carbon (C). If the main absorber is Pb, W or Ta, the selected combination for grading materials is Sn + Cu + Al + C. The characteristics of these elements are shown in Table 2.

Material	*Z*	*Density [g/cm3]*	*K_α energy [keV]*
Sn	50	7.31	25.37
Cu	29	8.96	8.05
Al	13	2.70	1.49
C	6	1.70	0.28

Table 2: Grading material characteristics.

For each grading layer, the thickness values are calculated in order to reach an efficiency *eff=99%* at the energy of the preceding K_α emission line.

Option A (I/I_0<1% at 40 keV) – Pb+Sn+Cu+Al+C:		*Option A (I/I_0<1% at 40 keV) – W+Sn+Cu+Al+C:*	
Pb thickness:	0.28 mm	W thickness:	0.224 mm
Sn thickness:	1.8 mm	Sn thickness:	0.96 mm
Cu thickness:	0.26 mm	Cu thickness:	0.26 mm
Al thickness:	0.34 mm	Al thickness:	0.34 mm
C thickness:	0.04	C thickness:	0.04 mm
Total thickness:	2.72 mm	Total thickness:	1.82 mm
Total column density:	1.97 g/cm^2	Total column density:	1.46 g/cm^2

Option A (I/I_0<1% at 40 keV) – Ta+Sn+Cu+Al+C:	
Ta thickness:	0.27 mm
Sn thickness:	0.79 mm
Cu thickness:	0.26 mm
Al thickness:	0.34 mm
C thickness:	0.03
Total thickness:	1.69 mm
Total column density:	1.35 g/cm^2

3. Shields design: a case study for the XEUS payload

Figure 2 shows the basic simplified geometry of the XEUS telescope assembly. The main quantities defined in Figure 2 and then used for the trade-off analysis are the following:

D_{opt}: External mirror shell diameter.
R_{skirt}: Skirt (MSC baffle) dimension, all around D_{opt}.
D_{MSC}: $D_{opt} + 2 \cdot R_{skirt}$
R_{MSC}: $D_{MSC}/2$
H: Collimator (DSC baffle) height.
D_{det}: Focal plane detector dimension.
s: Focal plane / collimator separation.
$\Delta\theta$: Detector opening angle, corresponding to Ω_{CXB} sr.
FL: Telescope focal length.

On the basis of the current feasibility scenarios, we have done the following assumptions:

D_{opt}: 420cm
R_{skirt}: Variable (technical feasibility to be assessed).
H: Variable (technical feasibility to be assessed).
D_{det}: Variable (depending on instruments FOV).
s: Large enough to avoid vignetting by the collimator walls (see below).
FL: 35m.

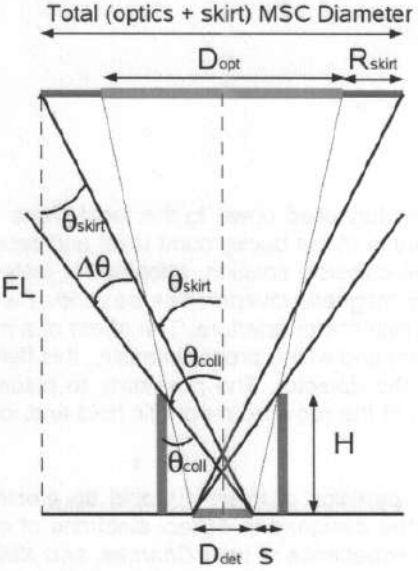

Figure 2:

The basic simplified geometry of the XEUS telescope assembly is shown. The **blue** horizontal line on the top indicates the external optics diameter, D_{opt}. The top external **green** lines represent the *skirt*, or MSC baffle, which adds a further R_{skirt} all around D_{opt}. The **purple** line on the bottom is the detection plane which has a dimension of D_{det} and is separated by s from the collimator (or DSC baffle) walls (**red** lines) of height H. FL is the telescope focal length.

Following a simple trigonometric approach we have that:

$$\Delta\theta = \theta_{coll} - \theta_{skirt} = \mathrm{arctg}\left[\frac{D_{det}}{H} + \frac{D_{opt} - D_{det}}{2 \cdot FL}\right] - \mathrm{arctg}\left[\frac{D_{MSC} + D_{det}}{2 \cdot FL}\right],$$

and therefore, putting $\Delta\theta=0$ (i.e. requiring a prefect shielding), we have:

$$D_{MSC} = 2 \cdot FL \cdot \left(\frac{D_{det}}{H} + \frac{D_{opt} - D_{det}}{2 \cdot FL}\right) - D_{det},$$

and

$$R_{skirt} = \frac{D_{MSC} - D_{opt}}{2}$$

We can now calculate the MSC skirt radius vs collimator height phase space that satisfies the requirement of a perfect shield for each of the XEUS instrument. The result is shown in Figure 3, that shows, for each XEUS instrument, the required skirt radius as a function of the collimator height in order to reach a perfect shielding, i.e. to shield against all directions outside the mirror shells.

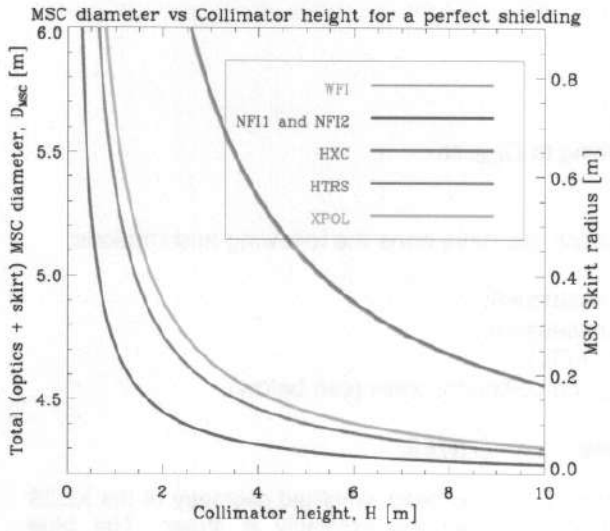

Figure 3:

Total MSC diameter (left Y axis) and skirt radius (right Y axis) as a function of the collimator height necessary to obtain a perfect shielding for each XEUS instrument.

4. Particle diverters study

Charged particles in the near-Earth environment can be funnelled down to the focal plane by the X-ray optics under certain circumstances, resulting in an increase of the background level and causing in some cases a decrease of the instruments performances. The classical solution, adopted for instance onboard *Chandra* and *XMM-Newton* to clean from electrons, is a magnetic diverter. The basic idea is quite simple and consists of a high magnetic field placed behind the rear mirror aperture. The effect of a magnetic field on a charged particle is to determine a change in direction and with a proper intensity, this field can deflect the electrons by an angle sufficient to avoid reaching the detector. The possibility to place it as far as possible from the detection plane allows a minimization of the required magnetic field and, consequently, of the mass budget.

It was believed for a long time that the only charged particles of interest would be electrons and the diverters onboard *Chandra*, *XMM-Newton*, and *Swift* were designed to deflect electrons of energy below the upper threshold of the detectors. However, after the experience of both *Chandra*, and *XMM-Newton*, it has been concluded that also protons with energies from few tens to several hundreds of keV can be funnelled by the optics down to the detection plane. In the case of *Chandra* this has resulted not only in a loss of science time but also in a damage to the detectors.

These effects triggered intensive study of the transmission of grazing-incidence protons through the *Chandra* and the *XMM-Newton* X-ray telescopes by using experiments with electrostatic accelerators and by means of computer simulations performed with Monte Carlo codes GEANT4 and MCNPX. Although simulations gave an underestimation of the scattering response function at very small angles, the main results are in a fair agreement with the experiments performed with the electrostatic accelerators and the in-flights measurements. All indicate the soft-protons as the main responsible of the observed damages. This prompted the search for measures in order to protect the CCDs from exposure to the space environment during passages through the radiation belts, where the largest concentration of low-energy protons are encountered. It was suggested that the detectors remain protected well beyond the extent of

radiation belts (about 40000 km) and are not exposed until the spacecraft reaches an altitude of about 70000 km. Presently, the observations starts when the geocentric distance is about 46000 km.
However, the soft-proton flares recorded during the observing time cannot be presently avoided. The onboard electron diverter can be somewhat effective for protons up to about 40 keV, not sufficient to prevent the incoming of the most dangerous population of protons (E>80 keV).

An electron diverter is relatively simple to design and implement, as shown by those onboard *Chandra*, *XMM-Newton*, and *Swift*. More difficult is to deflect protons, which have a mass 1839 times greater than electrons. However, since the radius of curvature ρ of a particle with mass *m*, charge *e* and energy *E* moving in a magnetic field of strength B, is:

$$\rho = \frac{1}{B}\sqrt{\frac{2Em}{e}},$$

which implies that the deflection should be improved only by a factor of $(m_p/m_e)^{1/2} \approx 40$.
In addition, in order to arrive onto the detector, the proton beam should be channelled tighter than an electron beam and, therefore, a smaller deflection angle is sufficient for protons to avoid the detectors. Another difference is that protons of a few tens of keV are sub-relativistic and lose much energy by ionization through filter and dead layers (observed energy is much less than proton energy on leaving the diverter), while electron energy remains approximately the same and electrons are easier to deflect.
To calculate the deflection angle θ, it is necessary to consider that deflection occurs only when the charged particle is in the magnetic field. Therefore, if *l* is the depth in the magnetic field, we have:

$$\theta = \arctan\left(\frac{l}{\rho}\right) = \arctan\left(Bl\sqrt{\frac{e}{2Em}}\right)$$

A recent ESA report (Ref II) demonstrates that required deflection angle depends also on the dimension of the beam of funnelled protons exiting the optics, which, at 1σ level and adopting the notation used in Ref II, can be expressed as follows (see Ref II for details):

$$\sigma_{p+beam} = \sqrt{\sigma^2_{FOV} + \sigma^2_{Scattering} + \sigma^2_{Reflection}}$$

For $\sigma_{Scattering}$ and $\sigma_{Reflection}$ (proton beam spreads due to the funnelling process) we adopt the values used in Ref II, while σ_{FOV} can be expressed as a function of the detector dimension, D_{Det}, and diverter-to-detector distance, *d*. In this way we have that:

$$\sigma_{p+beam} = \sqrt{\left(\frac{2}{2.36}\arctan\left(\frac{D_{Det}}{2d}\right)\right)^2 + \left(\frac{40'}{2.36}\right)^2 + \left(\frac{90'}{2.36}\right)^2}$$

We can then calculate the required magnetic field and depth, *lB* vs. the necessary deflection angle (assuming to require a 5σ confidence) which corresponds to a variable detector-to-deflector distance.

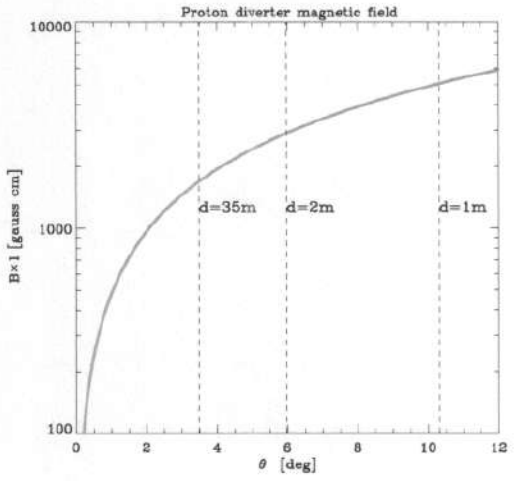

Figure 3:

Proton diverter magnetic field intensity, in gauss cm (Y axis), as a function of the required deflection angle (X axis), which increases for shorter diverter-to-detector distances.

References

I. Malaguti, G., et al. 2005, *"Active and passive shielding design optimization and technical solutions for deep sensitivity hard x-ray focusing telescopes"*, Optics for EUV, X-Ray, and Gamma-Ray Astronomy II. Edited by Citterio, O.; O'Dell, S. L. Proceedings of the SPIE, Volume 5900, pp. 159-171

II. ESA Document SCI-SA/AP/06/0412/cv, *"A Magnetic Diverter for Charged Particles on XEUS"*, April 2006

View publication stats